New Measurement of the $1S-3S$ Transition Frequency of Hydrogen: Contribution to the Proton Charge Radius Puzzle

Hélène Fleurbaey, Sandrine Galtier,* Simon Thomas, Marie Bonnaud, Lucile Julien, François Biraben, and François Nez
Laboratoire Kastler Brossel, Sorbonne Université, CNRS, ENS-Université PSL, Collège de France, 4 place Jussieu, Case 74, 75252 Paris Cedex 05, France

Michel Abgrall and Jocelyne Guéna
LNE-SYRTE, Observatoire de Paris, Université PSL, CNRS, Sorbonne Université, 61 avenue de l'Observatoire, 75014 Paris, France

(Received 8 December 2017; revised manuscript received 9 March 2018; published 4 May 2018)

We present a new measurement of the $1S-3S$ two-photon transition frequency of hydrogen, realized with a continuous-wave excitation laser at 205 nm on a room-temperature atomic beam, with a relative uncertainty of 9×10^{-13}. The proton charge radius deduced from this measurement, $r_p = 0.877(13)$ fm, is in very good agreement with the current CODATA-recommended value. This result contributes to the ongoing search to solve the proton charge radius puzzle, which arose from a discrepancy between the CODATA value and a more precise determination of r_p from muonic hydrogen spectroscopy.

DOI: 10.1103/PhysRevLett.120.183001

Hydrogen is a cornerstone of atomic physics, as it plays a key role in the determination of the Rydberg constant and in testing fundamental theories such as the quantum electrodynamics (QED) theory. Since it is the simplest atom, the energy levels of hydrogen are described theoretically with a good accuracy and can be written as the sum of two terms. The first term is directly linked to the Rydberg constant R_∞. It takes into account the solution of the Dirac equation and the leading-order recoil correction due to the finite mass of the proton. The second term, commonly known as the Lamb shift, includes QED and relativistic contributions, as well as the finite nuclear size effect characterized by the proton rms charge radius r_p. Hydrogen spectroscopy provides an access to differences of energy levels. For instance, the $1S-2S$ transition frequency has been measured with a relative uncertainty of 4.2×10^{-15} [1]. By making an appropriate linear combination of this frequency with that of another transition such as the $2S-nS/D$ transitions [2], one obtains experimental values of the Rydberg constant and of the ground-state Lamb shift, from which the proton radius can be derived, assuming that the QED calculations are correct. The global adjustment of fundamental constants realized by CODATA [3] partly relies on such a scheme, while also including deuterium spectroscopy and electron-proton or -deuteron scattering experimental results [4].

In 2010, the spectroscopy of muonic hydrogen [5,6] yielded a value of r_p an order of magnitude more precise, but about 4% smaller, than the CODATA-recommended value. This discrepancy has become known as the proton radius puzzle [7]. A recent measurement of the hydrogen $2S-4P$ transition frequency in Garching [8] has brought a new dimension to this conundrum, as it agrees with the smaller muonic value of the proton radius, in disagreement with other spectroscopic measurements in electronic hydrogen.

In this Letter, we present a new measurement of the $1S-3S$ two-photon hydrogen transition frequency, realized with a continuous-wave (cw) 205 nm excitation laser and detected through the Balmer-α $3S-2P$ fluorescence. For the first time, the uncertainty on this transition frequency (2.6 kHz) is significantly smaller than the proton radius discrepancy, which corresponds to a difference of 7 kHz for the $1S-3S$ transition frequency. This result improves previous measurements in Paris [9] as well as in Garching [10]. At this unprecedented level of precision, it will allow comparison with future results from the Garching experiment, which measures the same transition with an entirely different setup using a picosecond laser excitation.

The results presented in this Letter were obtained from data recorded in two separate sessions, in 2013 [11] and 2016–2017 [12]. Figure 1 presents a simplified view of the last version of the experimental setup. Our 205 nm cw excitation laser is produced by sum frequency generation (SFG), in a β-barium borate (BBO) crystal, of a homemade tunable titanium:sapphire (Ti:Sa) laser at 894 nm and a 266 nm radiation resulting from the frequency doubling of a 532 nm laser (Verdi V6 and MBD266, Coherent) [13]. This source delivers between 15 mW (in 2013) and 10 mW (in 2017) at 205 nm, depending on the BBO crystal quality and the SFG efficiency.

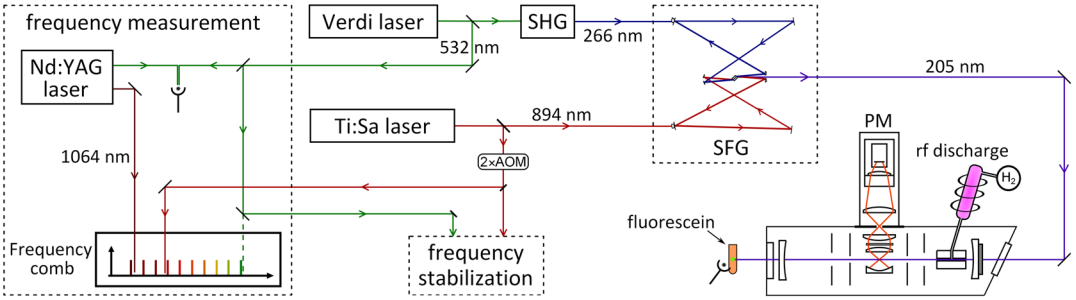

FIG. 1. Simplified view of the experimental setup. Frequency stabilization relies on several Fabry-Perot cavities and a Rb-stabilized standard laser. Since 2016, instead of making a beatnote directly with the frequency comb, the frequency of the Verdi laser is measured via a Nd:YAG transfer laser (more details in text). SHG: second harmonic generation, SFG: sum frequency generation, AOM: acousto-optic modulator, PM: photomultiplier.

The frequency stability of the Ti:Sa and Verdi lasers is ensured thanks to several Fabry-Perot cavities and a standard laser, a 778 nm laser diode stabilized on a two-photon hyperfine transition of ^{85}Rb [14,15]. A double-pass acousto-optic modulator (AOM) placed between the Ti:Sa laser and the frequency stabilization setup allows us to scan the excitation frequency while keeping all lasers stabilized.

The Ti:Sa and Verdi laser frequencies, at 894 nm and 532 nm, respectively, are measured by comparison with a MenloSystems femtosecond frequency comb, whose 780 nm output is spectrally broadened in a photonic crystal fiber (PCF). This frequency comb is referenced to the LNE-SYRTE Cs fountain primary frequency standards thanks to a 3-km-long optical fiber link [16]. In 2013, the recorded beatnote at 532 nm was weak because of the low power of the frequency comb at this wavelength. Since 2016, we have used an additional laser acting as a transfer laser. This cw Nd:YAG laser (Prometheus from Innolight) has two outputs: one at 532 nm, which is used to make a beatnote with our Verdi laser; the other at 1064 nm, whose frequency is measured through a beatnote with a new 1064 nm output of the frequency comb.

The frequency-stabilized 205 nm laser beam is injected into a power buildup cavity, whose axis is collinear with an effusive beam of H atoms formed by the dissociation of H_2 molecules in a radio-frequency discharge. The cavity mirrors have a 25 cm radius of curvature and are placed in a quasiconcentric configuration, yielding a waist radius of about 44 μm. The Balmer-α fluorescence photons are collected through a 656 nm interference filter and detected by a photomultiplier. The entire buildup cavity is inside a vacuum chamber, pumped by an oil diffusion pump. A liquid nitrogen trap reduces the oil vapor pressure in the spectroscopy chamber to negligible values. The pressure in the cavity is monitored by an ionization gauge placed on the side of the vacuum chamber, which only provides a relative measurement of the actual atomic flux. The stabilization of the buildup cavity is very sensitive to vibrations. In 2015, to improve the signal used for locking, we replaced the UV photodiode monitoring the transmitted light with a photodiode placed on the side of a quartz tube containing a fluorescein solution. Helmholtz coils, placed around the vacuum chamber, create the vertical magnetic field used for velocity distribution determination, as described below.

To observe the transition, we scan the frequency of the AOM placed in the Ti:Sa stabilization loop, following a predefined back-and-forth 31-point sequence to avoid drifts. For each AOM frequency point, we record the number of fluorescence photons collected by the photomultiplier during one second, as well as the various beatnote frequencies. A "signal" is obtained by averaging ten such scans. Figure 2 shows an average of 47 signals. We observe a rather large background, which is mainly due to UV-induced fluorescence of the detection optics.

The main systematic effect in our experiment is the second-order Doppler (SOD) effect, which is on the order of 135 kHz and depends on the atomic velocity distribution

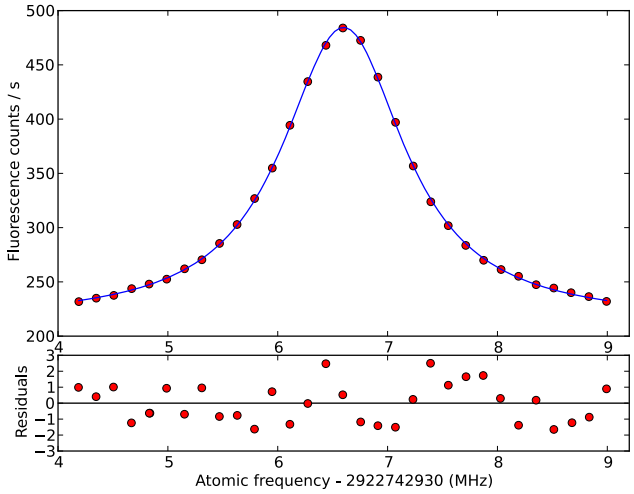

FIG. 2. Average of 47 recordings of the transition (four-hour integration time). No magnetic field was applied. Upper graph: The experimental data (red points) are fitted with a theoretical profile (blue line) calculated with the velocity distribution parameters $\sigma = 1.515$ km/s and $v_0 = 1.23$ km/s (see text). The observed linewidth is about 1.35 MHz, as compared to a natural width of 1 MHz. Lower graph: Residuals of the fit.

of our room-temperature effusive atomic beam. In order to determine this distribution, we follow a method detailed in Refs. [9,17], in which a vertical magnetic field **B** is applied in the interaction region, so that an atom moving with velocity **v** experiences a motional electric field $\mathbf{E} = \mathbf{v} \times \mathbf{B}$. The Stark shift due to this electric field has a quadratic velocity dependence, like the SOD shift. At the same time, the Zeeman effect lifts the degeneracy of the m_F hyperfine sublevels. The $1S_{1/2}^{F=1} - 3S_{1/2}^{F=1}$ transition splits into three components, in accordance with the two-photon selection rules ($\Delta m_F = 0$). The $m_F = 0$ component is greatly shifted by the Zeeman effect (about 10 MHz/mT for a magnetic field around 18 mT) and is used to calibrate the magnetic field. The two other components are, in first approximation, not shifted by the Zeeman effect. For a magnetic field of about 18 mT, a level crossing occurs between the $3S_{1/2}(F = 1, m_F = -1)$ and $3P_{1/2}(F = 1, m_F = 0)$ levels. The motional Stark shift is then large for the $m_F = -1$ component and could compensate the SOD shift for this particular subtransition. But the $m_F = \pm 1$ components of the transition are not resolved, since both the SOD and Stark shifts are an order of magnitude smaller than the natural width of the transition (1 MHz). Thus, the SOD shift is only partly compensated. We record the transition signal for no applied magnetic field (residual field of 0.03 mT) and for different values of the magnetic field around the level crossing. To avoid bias due to a possible stray electric field, we also reverse the magnetic field direction. Figure 3 shows the apparent line position ν_A, obtained by fitting the line with a simple Lorentzian shape, when the magnetic field is swept around the level crossing.

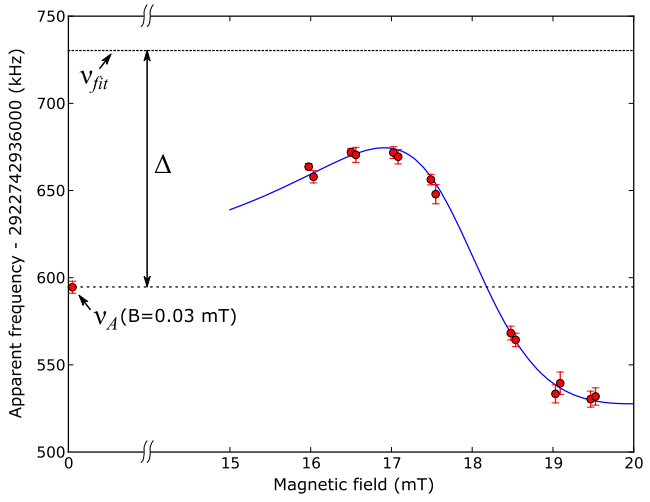

FIG. 3. Experimental (red circles) and calculated (blue curve) apparent positions of the $1S - 3S$ signal as a function of the applied magnetic field B. Each position is given by the center of the best-fitting Lorentzian curve of the experimental or the calculated profile at this B value. The parameters of the velocity distribution used to obtain the blue curve are the ones deduced from the analysis of the LP2 set of data (see below): $\sigma = 1.495$ km/s and $v_0 = 1.33$ km/s.

The analysis relies on a theoretical line profile described elsewhere [9], which includes the SOD and motional Stark shifts. Using the density matrix formalism, it involves summing the fluorescence of the $3S(F = 1, m_F = 0, \pm 1)$ sublevels and that of the $3P$ levels to which they can be coupled by the motional Stark effect. The $m_F = 0$ component only contributes to the signal for a null applied magnetic field. The profile is then integrated over a given atomic velocity distribution. Our velocity distribution model,

$$f(v, \sigma, v_0) \propto v^3 e^{-v^2/(2\sigma^2)} P(v/\sigma) e^{-v_0/v}, \qquad (1)$$

is based on the Maxwellian-type distribution of an effusive beam ($\sigma = \sqrt{kT/M}$, temperature T, atomic mass M) [18] and includes the correction $P(v/\sigma)$, which describes a depletion of slow atoms due to interactions within the nozzle [19]. It is multiplied by an exponential decay term to modelize a possible additional depletion of the slow atoms in the effusive beam. This distribution is fully described by the two parameters σ and v_0 [15]. Moreover, the profile is convoluted with a Lorentzian function to take into account broadening effects, mainly due to transit time and pressure broadenings.

The first recording session in 2013, lasting 29 days, yielded 1019 signals recorded for a pressure of 7.5×10^{-5} mbar and 7 magnetic field values. Subsequently, after improving the frequency measurement setup, a second recording session was undertaken during 59 days (1700 signals) in 2016–2017. This time, the magnetic field procedure was applied for two different pressure values (2.7×10^{-5} and 2×10^{-4} mbar), in order to characterize a possible pressure dependence of the velocity distribution. For analysis, we separated the 2016 data into three sets: two sets at low pressure (LP1, LP2) recorded before and after the high-pressure set (HP). Unfortunately, the pressure gauge was replaced between the two recording sessions, so the indicated pressure values are not comparable between 2013 and 2016–2017.

The four data sets were analyzed independently to determine the velocity distribution parameters, through a chi-square minimization process. Each signal is fitted by theoretical profiles calculated for a grid of (σ, v_0) parameters, to determine its center frequency. The other fit parameters are the amplitude, background offset, and Lorentzian broadening width. For a given data set, the mean frequency and the chi-square χ^2 are computed. The best-fitting velocity distribution parameters are given by the minimum of the $\chi^2(\sigma, v_0)$ surface fitted by a polynomial function. The results of this minimization for the various data sets are given in the first two lines of Table I. Eventually, the signals are fitted again using the theoretical profile calculated for the best-fitting velocity distribution. The average of this set gives the optimal frequency ν_{fit}, which takes into account the SOD, the Zeeman effect, and the motional Stark shifts.

TABLE I. Optimal velocity distribution parameters σ and v_0 and determination of the $1S-3S(F=1)$ frequency. ν_A is the apparent position of the line for $B=0.03$ mT, and Δ is the difference between the result of the fit procedure ν_{fit} and ν_A. It corresponds essentially to the SOD [for $B=0.03$ mT, the Zeeman shift of the $1S-3S(F=1)$ frequency is 1.0 kHz]. Δ_{LS} is the light-shift correction, ν_{LS} the light-shift-corrected frequency, Δ_p the pressure correction, $\nu_{\mathrm{LS},p}$ the frequency corrected from the light and pressure shifts, and Δ_{cd} the cross-damping effect. Δ_{maser} comes from the absolute calibration of the 100 MHz signal used as frequency reference. Only the last four digits of the $1S-3S(F=1)$ frequency are given in the table: $\nu = 2\,922\,742\,936\mathrm{xxx.x}$ kHz.

Data set	2013	LP1	LP2	HP
σ (km/s)	1.526(27)	1.515(52)	1.495(32)	1.521(85)
v_0 (km/s)	0.75(28)	1.23(55)	1.33(31)	0.87(78)
ν_A (kHz)	592.2(0.7)	596.8(0.9)	594.4(1.1)	581.6(2.2)
Δ (kHz)	132.6(1.3)	137.4(3.8)	135.9(2.1)	131.6(6.8)
ν_{fit} (kHz)	724.8(1.5)	734.2(3.9)	730.3(2.4)	713.2(7.1)
Δ_{LS} (kHz)	−5.9(1.2)	−10.4(3.0)	−12.1(3.6)	−6.3(10.2)
ν_{LS} (kHz)	718.9(1.9)	723.8(4.9)	718.2(4.3)	706.9(12.4)
Δ_p (kHz)	3.6(2.0)	Pressure extrapolation		
$\nu_{\mathrm{LS},p}$ (kHz)	722.5(2.8)	722.3(4.9)		
Δ_{cd} (kHz)	0.6(0.2)	0.6(0.2)		
Δ_{maser} (kHz)	−0.599(6)	−1.043(6)		
$\nu_{1S-3S}^{(F=1)}$	722.5(2.8)	721.9(4.9)		

To take into account the light shift, we apply to each signal a frequency correction based on a parameter indicating the intracavity power (see the Supplemental Material at Ref. [20] for more details). Two such parameters have been used: the voltage of the photodiode recording the transmitted UV power (for the 2013 recordings) and the square root of the two-photon absorption signal height (for 2016–2017). As the signal height depends on pressure, the correction coefficient was determined separately for each pressure value. The Δ_{LS} correction is obtained by a linear extrapolation of the frequency with respect to the chosen parameter. The light-shift-corrected frequencies ν_{LS} are given in Table I.

Collisions between atoms can also induce frequency shifts, depending linearly on the pressure. To determine this pressure shift for the 2013 data set, measurements were carried out several times during that recording session, for two or three pressure values in the same day, with no applied magnetic field. At that time, the velocity distribution was measured for only one pressure value, and our velocity distribution model could allow for pressure dependence of the parameter v_0, so we did not know which parameters should be used to analyze the other pressure points [15]. The analysis of the 2016 data gave us insight on this question. In fact, the velocity distribution does not seem to depend significantly on pressure, at least within experimental uncertainties (see Table I). To check this assumption, we have fitted a number of signals using the various best-fitting distributions. The resulting change in the center frequency was at most about 3 kHz. Hence, when analyzing the 2013 recordings, we use the same velocity distribution for all pressure values, and we add in quadrature an uncertainty of 3 kHz for the points measured at a pressure different from 7.5×10^{-5} mbar. We thus get a pressure correction of $+3.6(2.0)$ kHz (see Table I). For the 2016–2017 session, since the velocity distribution was determined for each pressure value, we simply extrapolate the light-shift-corrected frequencies of the three data sets to zero pressure.

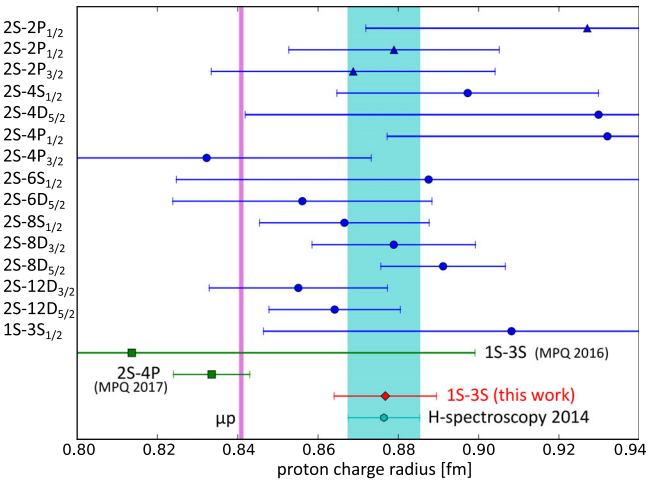

FIG. 4. Proton charge radius values from H spectroscopy, with 1σ error bars. The pink bar is the value from muonic hydrogen spectroscopy [6]. The CODATA-2014 H-spectroscopy average [3] (light blue bar and hexagon) includes RF measurements (blue triangles) as well as combinations of optical transitions with the $1S-2S$ frequency (blue circles). Green squares are obtained from optical transitions measured in Garching since 2014 [8,10], and the red diamond is the present work.

At this point, we add a correction of $+0.6(0.2)$ kHz to take into account the frequency shift resulting from the cross-damping effect [22,23], following our theoretical estimation of this shift [24].

All the frequency measurements were done with respect to the 100 MHz reference signal from LNE-SYRTE. This reference was obtained from a hydrogen maser, whose frequency was continuously measured by the LNE-SYRTE atomic fountains realizing the frequency of the SI second to a few 10^{-16} [25,26]. Using a simple linear frequency drift of the order of 10^{-16} per day to model the H-maser behavior over each period, we estimate the average fractional shift of the reference signal with respect to the SI to be $-205(2)\times10^{-15}$ in 2013, and $-357(2)\times10^{-15}$ in 2016–2017. This yields an absolute correction to the $1S-3S$ transition frequency of $-599(6)$ Hz for the 2013 measurement and $-1043(6)$ Hz for the 2016–2017 measurement.

The centroid value of the transition is calculated by adding a hyperfine correction of $+341\,949.077(3)$ kHz derived from experimental values of the $1S$ and $2S$ hyperfine splittings [27]. Eventually, we obtain for the two recording sessions

$$\nu_{1S-3S}^{2013} = 2\,922\,743\,278\,671.6(2.8)\ \text{kHz}, \quad (2)$$

$$\nu_{1S-3S}^{2017} = 2\,922\,743\,278\,671.0(4.9)\ \text{kHz}. \quad (3)$$

We estimate a correlation coefficient of 0.186 between the two results. The weighted average of our two measurements is then $\nu_{1S-3S} = 2\,922\,743\,278\,671.5(2.6)$ kHz. Combining this result with the $1S-2S$ transition frequency [1], one can derive values of the Rydberg constant, $R_\infty = 10\,973\,731.568\,53(14)\ \text{m}^{-1}$, and the proton charge radius, $r_p = 0.877(13)$ fm. The latter is shown in Fig. 4 along with other determinations of the proton radius from hydrogen spectroscopy. The present result is in very good agreement with the CODATA-2014 recommended value [0.8751(61) fm [3]], and disagrees with the value deduced from muonic spectroscopy [6] by 2.8σ, thus reinforcing the proton radius puzzle.

In the near future, we plan to cool the hydrogen beam down to the temperature of liquid nitrogen, in order to reduce the second-order Doppler shift and improve the accuracy of our measurement.

The authors thank O. Acef for the transfer laser. This work was supported by the French National Research Agency (ANR) through the cluster of excellence FIRST-TF (ANR-10-LABX-48), the PROCADIS project (ANR-2010-BLANC:04510) and the Equipex REFIMEVE+ (ANR-11-EQPX-0039), and by the CNRS.

*Present address: Institut Lumière Matière, UMR 5306 Université Lyon 1-CNRS, Université de Lyon, 69622 Villeurbanne Cedex, France.

[1] C. G. Parthey *et al.*, Phys. Rev. Lett. **107**, 203001 (2011).
[2] B. de Beauvoir, C. Schwob, O. Acef, L. Jozefowski, L. Hilico, F. Nez, L. Julien, A. Clairon, and F. Biraben, Eur. Phys. J. D **12**, 61 (2000).
[3] P. J. Mohr, D. B. Newell, and B. N. Taylor, Rev. Mod. Phys. **88**, 035009 (2016).
[4] J. Arrington and I. Sick, J. Phys. Chem. Ref. Data **44**, 031204 (2015).
[5] R. Pohl *et al.*, Nature (London) **466**, 213 (2010).
[6] A. Antognini *et al.*, Science **339**, 417 (2013).
[7] C. E. Carlson, Prog. Part. Nucl. Phys. **82**, 59 (2015).
[8] A. Beyer *et al.*, Science **358**, 79 (2017).
[9] O. Arnoult, F. Nez, L. Julien, and F. Biraben, Eur. Phys. J. D **60**, 243 (2010).
[10] D. C. Yost *et al.*, Phys. Rev. A **93**, 042509 (2016).
[11] S. Galtier, Ph.D. thesis, Université Pierre et Marie Curie, 2014, https://hal.archives-ouvertes.fr/tel-01080669.
[12] H. Fleurbaey, Ph.D. thesis, Université Pierre et Marie Curie, 2017, https://hal.archives-ouvertes.fr/tel-01633631.
[13] S. Galtier, F. Nez, L. Julien, and F. Biraben, Opt. Commun. **324**, 34 (2014).
[14] D. Touahri, O. Acef, A. Clairon, J.-J. Zondy, R. Felder, L. Hilico, B. de Beauvoir, F. Biraben, and F. Nez, Opt. Commun. **133**, 471 (1997).
[15] S. Galtier, H. Fleurbaey, S. Thomas, L. Julien, F. Biraben, and F. Nez, J. Phys. Chem. Ref. Data **44**, 031201 (2015).
[16] B. de Beauvoir, F. Nez, L. Hilico, L. Julien, F. Biraben, B. Cagnac, J.-J. Zondy, D. Touahri, O. Acef, and A. Clairon, Eur. Phys. J. D **1**, 227 (1998).
[17] G. Hagel, R. Battesti, F. Nez, L. Julien, and F. Biraben, Phys. Rev. Lett. **89**, 203001 (2002).
[18] N. F. Ramsey, *Molecular Beams* (Oxford University Press, New York, 1956).
[19] D. R. Olander, R. H. Jones, and W. J. Siekhaus, J. Appl. Phys. **41**, 4388 (1970).
[20] See Supplemental Material at http://link.aps.org/supplemental/10.1103/PhysRevLett.120.183001 for more details on the light shift and pressure shift, which includes Ref. [21].
[21] J. W. Farley and W. H. Wing, Phys. Rev. A **23**, 2397 (1981).
[22] M. Horbatsch and E. A. Hessels, Phys. Rev. A **82**, 052519 (2010).
[23] M. Horbatsch and E. A. Hessels, Phys. Rev. A **84**, 032508 (2011).
[24] H. Fleurbaey, F. Biraben, L. Julien, J.-P. Karr, and F. Nez, Phys. Rev. A **95**, 052503 (2017).
[25] J. Guéna *et al.*, IEEE Trans. Ultrason. Ferroelectr. Freq. Control **59**, 391 (2012).
[26] G. D. Rovera, S. Bize, B. Chupin, J. Guéna, P. Laurent, and P. Rosenbusch, Metrologia **53**, S81 (2016).
[27] S. G. Karshenboim and V. G. Ivanov, Eur. Phys. J. D **19**, 13 (2002).